Bulletin of Electrical Engineering and Informatics
Vol. 14, No. 6, December 2025, pp. 4900~4912
ISSN: 2302-9285, DOI: 10.11591/eei.v14i6.10425

Load frequency control of multi-source power system using PID+DD controller based on chess algorithm

Chatmongkol Areeyat[1], Sittihsak Audomsi[1], Jagraphon Obma[2], Xiaoqing Yang[3], Worawat Sa-ngiamvibool[1]
[1]Electrical and Computer Engineering Research Unit, Faculty of Engineering, Mahasarakham University, Maha Sarakham, Thailand
[2]Department of Computer Engineering, Rajamangala University of Technology ISAN, Khonkaen Campus, Khonkaen, Thailand
[3]Shanxi Vocational University of Engineering Science and Technology, Shanxi, China

Article Info

Article history:

Received Apr 8, 2025
Revised Sep 4, 2025
Accepted Sep 27, 2025

Keywords:

Chess algorithm
Hydro-thermal
Load frequency control
Multi-source power system
Proportional–integral–derivative plus second controller
Wind power energy

ABSTRACT

This article presents load frequency control for a nonlinear multi-source power system divided into three areas, consisting of thermal reheat power plants, hydropower, and wind generation, while considering generation rate constraints (GRC). A proportional–integral–derivative (PID) plus second-order derivative (PID+DD) controller optimized using the chess algorithm (CA) is proposed. The effectiveness of CA is validated against hippopotamus optimization (HO), grey wolf optimizer (GWO), and ant lion optimizer (ALO) under two scenarios: a 10% step load perturbation (SLP) and a random load pattern (RLP). Simulation results indicate that the proposed CA significantly improves dynamic performance. In scenario 1 (10% SLP), CA achieves a reduction of approximately 30.5% in integral weight time absolute error (ITSE) compared to GWO and 43.7% compared to HO, while also reducing frequency undershoot in Area 2 by 15.2% compared to HO. In scenario 2 RLP, CA maintains robustness, limiting tie-line power deviations to ±8 MW, whereas HO exhibits deviations exceeding ±12 MW. Overall, the CA-tuned PID+DD controller demonstrates superior damping, reduced overshoot and undershoot, and enhanced stability across multi-area interconnected renewable systems, making it a promising approach for future real-time load frequency control (LFC) applications with higher renewable penetration.

Corresponding Author:

Worawat Sa-ngiamvibool
Electrical and Computer Engineering Research Unit, Faculty of Engineering, Mahasarakham University
Maha Sarakham 44150, Thailand
Email: wor.nui@gmail.com

1. INTRODUCTION

The increasing integration of renewable energy sources into modern power systems has introduced significant operational challenges due to their inherent intermittency and unpredictability. The interaction of nonlinear and dynamic load demands leads to ongoing oscillations in system frequency and tie-line power, potentially causing instability or system failure. Automatic generation control (AGC) plays a crucial role in addressing these issues by managing frequency and tie-line power within acceptable limits [1]. In AGC, load frequency control (LFC) plays a crucial role in ensuring stable and reliable interconnected operations [2].

Previous studies on LFC can be broadly categorized into single-source, two-source, and multi-source systems [3]. Raju *et al*. [4] conducted an examination of a three-area thermal power plant with generation rate constraints (GRC) and introduced a proportional–integral–derivative (PID) plus second-order derivative PID+DD controller, showcasing improved performance compared to traditional I, PI, and PID

controllers. Sitthisak Audomsi modified controller parameters for a two-area thermal power plant using the chess algorithm (CA), leading to improvements in overshoot, undershoot, and settling time compared to particle swarm optimization (PSO). Further research [5]-[9] has examined AGC in hybrid systems that incorporate wind energy, often simulating stochastic wind speed profiles to reflect real-world variability. This research has confirmed that CA offers competitive convergence attributes and solution quality due to its diverse search strategies based on chess piece movements.

Despite these advancements, several gaps remain. Many contemporary studies focus on single- or dual-area systems, with minimal attention given to multi-source topologies that integrate thermal, hydro, and renewable resources within real operational constraints. Moreover, while CA has shown effectiveness, its application in multi-source LFC scenarios—particularly alongside hybrid control methods such as PID+DD—has not been thoroughly investigated. Critical elements, such as the ability to withstand sudden load changes and the variability associated with renewable energy sources, remain insufficiently explored.

This paper offers a PID+DD controller, optimized using the CA, to overcome the deficiencies in LFC inside a multi-source power system. The principal contributions are:

- Development of a multi-source load frequency control model that integrates actual generation rate limitations and renewable variability.
- Implementation of a cellular automaton-based parameter optimization framework for the PID+DD controller.
- Comparative assessment against alternative metaheuristic algorithms to illustrate enhancements in integral weight time absolute error (ITSE), overshoot, and undershoot measurements.
- Evaluation of robustness under several operational situations.

The following sections of the paper are organized as outlined below: section 2 outlines the system model and the architecture of the controller, describes the CA and its integration with the PID+DD controller, and presents the simulation configuration and experimental settings. Section 3 reports the findings and provides a comparative analysis with recognized methodologies. Finally, section 4 concludes the study and suggests potential directions for future research.

2. METHOD

2.1. System investigated

Figure 1 shows the operations for each zone within the frequency fluctuation of the 50 Hz electricity system. In Zone A, disconnecting from power generation is unnecessary when the variation surpasses Zone 1, which is within acceptable limits. This zone is called the Prohibited trip Zone. If there is a frequency variation from the normal value in Zone B, it is mandatory to disconnect the power generation. This applies when the frequency variation is 1% within 11 minutes, 2.5% within 1.5 minutes, 4% within 10 seconds, and 5% within 5 seconds. This zone is called the Permitted trip Zone. Zone C, also known as the instantaneous trip zone, requires immediate release. Thermal power plants use it in Zone D. If there is a frequency variation of 2.5%, the power generation must be reduced within 1.5 minutes, and if there is a frequency variation of 2.83%, it must be reduced within 2 seconds. The consumer electrical equipment can endure frequency variations up to ±0.5 Hz or approximately ±1% for a 50 Hz electrical system according from IEEE 446-1995 standard specifies [10].

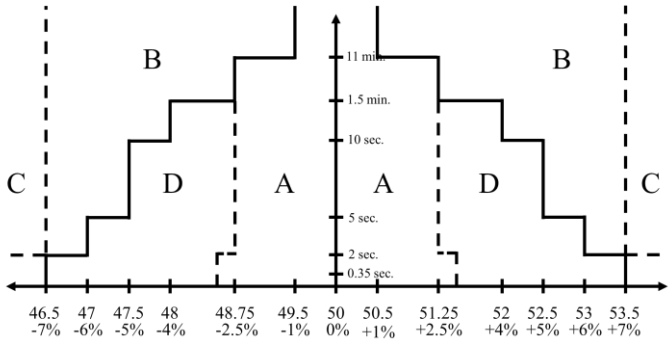

A : Trip prohibited
B : Trip permitted
C : Trip Instantaneous
D : Trip permitted for Thermal power plants

Figure 1. Frequency deviation zones

Multi-source power plants in this context consist of the interconnected of thermal reheat power plants, thermal reheat power plants with wind turbine generators, and hydropower plants with wind turbine generators. The generation rates are 1000 MW for Area 1, 2000 MW for Area 2, and 4000 MW for Area 3, or in a ratio of 1:2:4. The thermal reheat power plants have a maximum GRC of 5% per minute, and the hydropower plants have a maximum GRC of 370% per minute, as shown in Figure 2: in Figure 2(a) for Area 1, Figure 2(b) for Area 2, and Figure 2(c) for Area 3. All parameter values specified in the transfer function of the power system will be presented in Table 1 and Appendix A. The study used a PID plus second-order derivative controller [4], where the controllers are independent in each area, and different algorithms such as hippopotamus optimization (HO) [11], grey wolf optimizer (GWO) [12], ant lion optimizer (ALO) [13], and CA [14] are used to find the parameters.

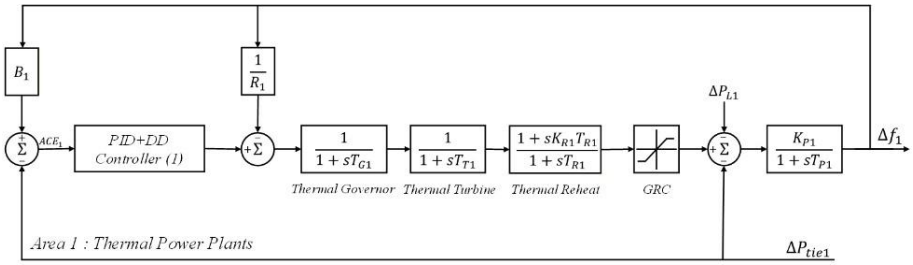

(a)

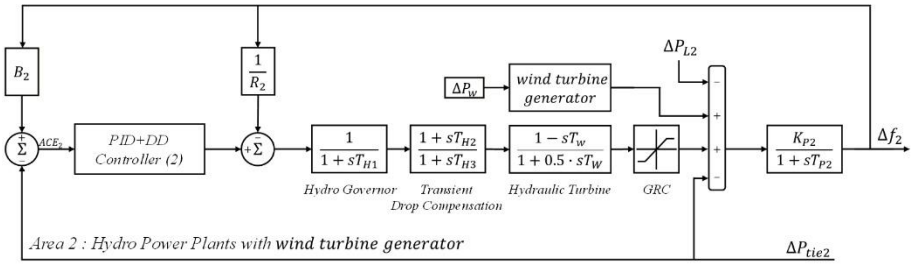

(b)

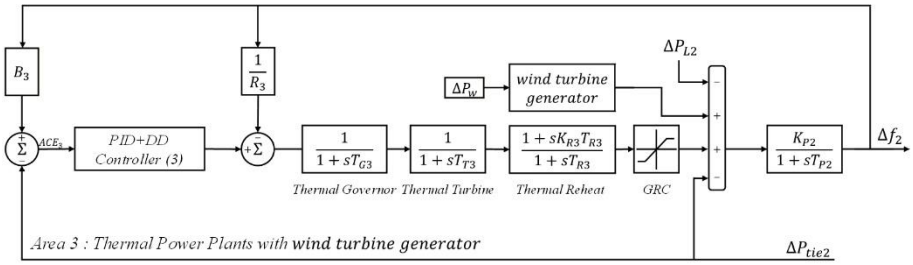

(c)

Figure 2. Block diagrams of the three-area multi-source power system with PID+DD controllers: (a) thermal power plant in Area 1, (b) hydropower plant and wind turbine generator in Area 2, and (c) thermal power plant and wind turbine generator in Area 3

In considering scenario cases, in Figure 3, step load perturbation (SLP) and random load pattern (RLP) [15] in Area 1 are shown in Figures 3(a) and (b), respectively. the optimal value is determined from the objective function or the best cost function, which in this case is the ITSE represented by [1]. The simulation and testing will be conducted using MATLAB/Simulink.

$$\text{ITSE} = \int_0^{t_{sim}} t \cdot \{(\Delta f_i)^2 + (\Delta P_{tie-i})^2\} dt \quad (1)$$

Where i is area number.

The ACE signal, a positive feedback loop consisting of components, is used to control power transmission fluctuations through tie-line (ΔP_{tie}). Control the frequency (Δf_i) of the electrical system when interconnected as shown in (2) and ACE as shown in (3):

$$\Delta P_{tie,i} = 2\pi \left[\sum_{\substack{j=1 \\ j \neq i}}^{N} T_{ij}\Delta f_i - \sum_{\substack{j=1 \\ j \neq i}}^{N} T_{ij}\Delta f_j \right] \quad (2)$$

$$ACE_i = B \cdot \Delta f_i + \Delta P_{tie,i} \quad (3)$$

Table 1. The parameters of wind turbine generation

Area 2		Area 3	
Parameters	Value	Parameters	Value
ρ	1.225 kg/m^3	ρ	1.225 kg/m^3
R_T	52 m	R_T	52 m
β	5 degree	β	5 degree
$P_{W,max}$	10 MW	$P_{W,max}$	10 MW
n_r	10 rpm	n_r	10 rpm
V_W	12 m/s	V_W	15 m/s
ϕ_1	-0.6175	ϕ_1	-0.6175
ϕ_2	116	ϕ_2	116
ϕ_3	0.4	ϕ_3	0.4
ϕ_4	0	ϕ_4	0
ϕ_5	5	ϕ_5	5
ϕ_6	21	ϕ_6	21
ϕ_7	0.1405	ϕ_7	0.1405

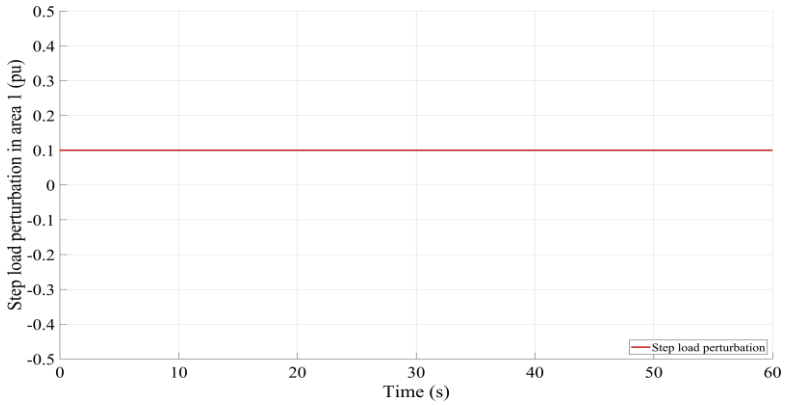

(a)

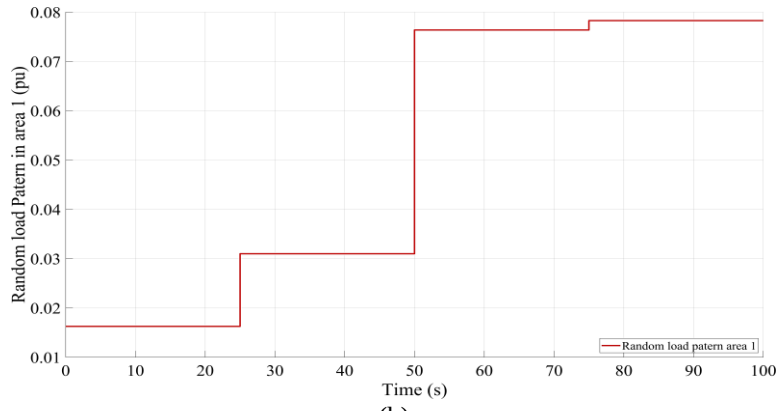

(b)

Figure 3. Load disturbance scenarios applied in the three-area multi-source power system: (a) step load perturbation and (b) random load pattern

2.2. Proportional–integral–derivative plus second-order derivative controller

The PID controller plus second-order derivative [4] is an extension of the PID controller's functionality by incorporating the second-order derivative into the control system, as shown in the Figure 4. To better handle sudden changes and the speed-up of system errors, adding second-order derivatives will help

lower the problems of volatility and oscillation that can come up because the system's response isn't stable, especially when there are outside stimuli or changes. The application of second-order derivatives enables the controller to assess the rate of error variation with greater precision, facilitating a more rapid and stable system response. The method is appropriate.

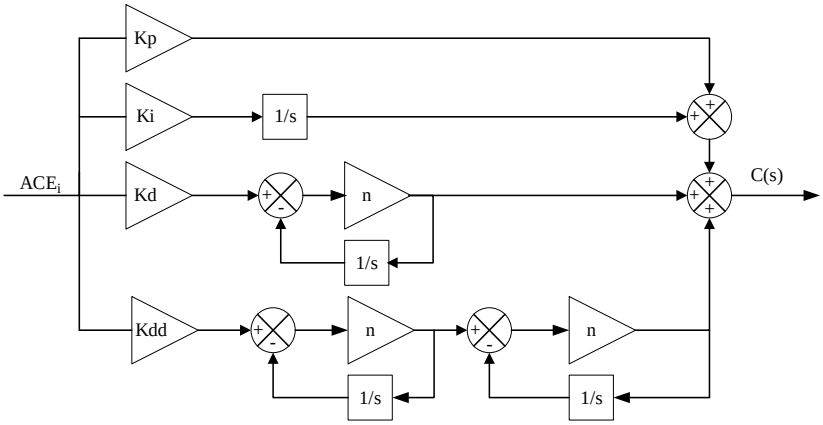

Figure 4. Structure of PID plus second-order derivative

2.3. System and model configuration

2.3.1. Thermal power plants

Modeling thermal power plants with reheat consists of three main components: the governor, the steam turbine, and the reheater. In practice, all components are nonlinear and constrained by GRC. Documents [16]-[18] contain the transfer function descriptions for each component of the thermal power plant. These can be summarized by (4):

$$G_{theraml}(s) = \left[\frac{1}{1 + sT_G}\right]\left[\frac{1}{1 + sT_T}\right]\left[\frac{1 + sK_R T_R}{1 + sT_R}\right] \quad (4)$$

2.3.2. Hydropower plants

Modeling of hydropower plants consists of three main components: the hydraulic governor, the drop compensation, and the hydraulic turbine. In [19]-[23] have explained the details of the transfer function and can summarize it as (5).

$$G_{Hydro}(s) = \left[\frac{1}{1 + sT_{H1}}\right]\left[\frac{1 + sT_{H2}}{1 + sT_{H3}}\right]\left[\frac{1 - sT_W}{1 + 0.5sT_W}\right] \quad (5)$$

2.3.3. Wind power generation

The wind turbine power generation system is characterized by discontinuity and nonlinearity, attributable to the inherently variable nature of wind energy, which experiences constant fluctuations in wind speed. A model of fluctuating wind speed is created using MATLAB/Simulink in accordance with the specified design. The random noise is multiplied by the wind velocity, in Figure 5 shown with the result obtained from a white noise block [24]-[26].

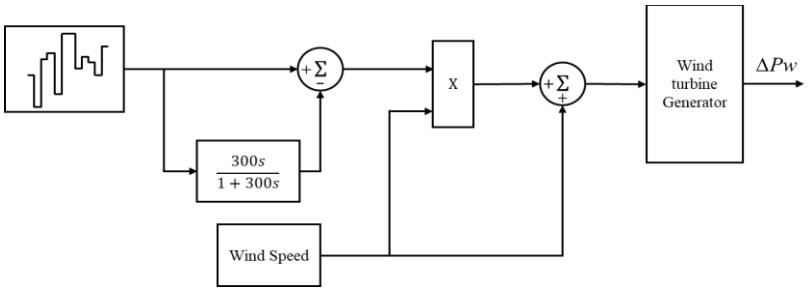

Figure 5. Wind power generation source model

In (6) is shown as a transfer function, which describes how the system works for controlling wind energy in a wind turbine generator (WTG) [24] or how a wind energy generator responds as a first-order transfer function.

$$G_{WTG}(s) = \left[\frac{K_{WTG}}{1 + sT_{WTG}} \right] \quad (6)$$

The electrical energy produced by the wind turbine is represented by (7), where P_W is the energy produced by the wind turbine (W), V_W is the wind speed (m/s), ρ is the air density (kg/m³), A_T is the cross-sectional area of the blades (m²), and ϕ_1-ϕ_7 are the coefficients used in calculating the value of C_P.

$$P_W = \frac{1}{2}\rho A_T V^3 C_p(\lambda,\beta) \quad (7)$$

The characteristic of the wind turbine is that when the wind speed changes, the pitch angle of the blades also changes accordingly, resulting in non-linearity. The optimum tip-speed ratio (TSR), defined as the ratio of the speed at the tip of the blades to the wind speed (λ_T), is represented by (8):

$$\lambda_T = \frac{\omega_T \cdot R_T}{V_W} \quad (8)$$

where R_T is the radius of the blade and ω_T is the angular velocity of the blade.

In situations where wind speed varies, variable-speed wind turbines function at the optimal tip speed ratio (λ_i) rather than the fluctuating tip speed ratio, which can be calculated using (9):

$$\frac{1}{\lambda_i} = \frac{1}{\lambda_T + 0.08\beta} - \frac{0.035}{\beta^3 + 1} \quad (9)$$

The power coefficient is the ratio of the blade's tip speed to its pitch angle. The approximation is determined by a function defined in (10):

$$C_P(\lambda,\beta) = \phi_1\left(\frac{\phi_2}{\lambda_i} - \phi_3\beta - \phi_4\beta^2 - \phi_5\right) \cdot e^{-\frac{\phi_6}{\lambda_i}} + \phi_7\lambda_T \quad (10)$$

Calculating the parameters, it was found that the energy output shown in Figure 6(a) for area 2 and Figure 6(b) for area 3 is not constant due to the non-linear nature of the speed, which changes continuously. Therefore, the produced energy is neither stable nor constant.

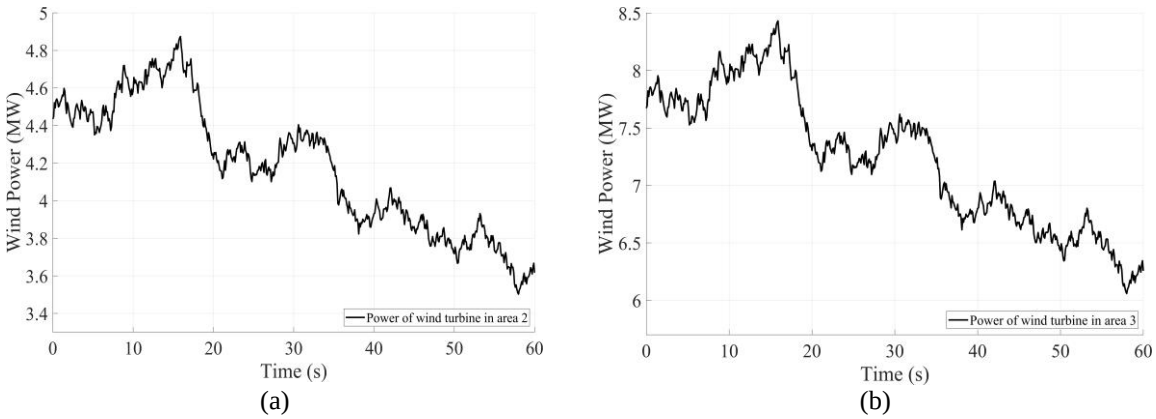

(a) (b)

Figure 6. Wind power profiles in multi-area system: (a) Area 2 and (b) Area 3

2.4. Chess algorithm

Chess is a historical board game that is very ancient and dates back thousands of years. It is among the world's most popular strategy games. Chess, however, is all about planning and anticipation, along with a perceptive understanding of situations. It is the balancing of one's offense and defense. Modern international chess is played by two opponents against each other with 16 pieces each: 1 King, 1 Queen, 2 Rooks, 2 Knights, 2 Bishops, and 8 Pawns, with the objective of checkmating the king of the opponent. Some fundamental moves for every piece are as follows: the king may traverse to any adjacent square, moving

vertically, horizontally, or diagonally; the queen can traverse in any direction, including linear and diagonal; the rook advances in a straight line; the bishop progresses diagonally; the knight maneuvers in an "L" shape; and the pawn advances one square forward while capturing diagonally. The way rules dictate which game pieces move leads to better search efficiency for optimal value. The process of the chess algorithm is as:
Step 1. Set the population's initialization to Np=8 and set the iteration.
Step 2. Calculate the objective function for each piece and then rank the answers from the best to the worst.
Step 3. Replace the ordered answers with different types of pawns, starting with kings, queens, rooks, knights, bishops, and pawns.
Step 4. Let each piece search for answers in the surrounding area according to the movement pattern of each type of pawn.
Step 5. Find the value of the function for each answer and determine the best value around each type of pawn.
Step 6. Move each type of pawn to the best answer found.
Step 7. Compare the answers from the search and select the best one.
Step 8. Check the stop conditions.
Step 9. Give 8 pawns, randomly find a new initial answer, and calculate the function value of the answer.
Step 10. Take the best answers of the 8 pawns and the answers that start anew from all pawns, sort them from the best answers, and select the top 8.

3. RESULTS AND DISCUSION

The performance of the HO, GWO, ALO, and CA algorithms was compared to find the best parameter for the PID+DD controller, looking at two scenarios: one with a 10% SLP in Area 1 of the multi-source power system. The results are shown in Table 2. Figure 7 shows the response under a 10% SLP load, and case 2 in Figure 8 shows the response under RLP. Parameter values are shown in Table 3. The analysis in the first case revealed that CA could accurately determine the parameters, yielding the best undershoot results for frequency deviation.

3.1. Scenario 1: 10% step load perturbation

Scenario 1 uses 10% SLP from Table 2, the overshoot at Δf1 using GWO is 0.21501, which is slightly higher than CA (0.21510), but GWO achieves a lower undershoot (−0.11637 vs −0.11498 of CA). At Δf2, the CA method provides the minimum undershoot (−0.05949) compared to HO (−0.07019) and ALO (−0.06467), showing about 15.2% improvement over HO. Similarly, at ΔPtie,1 the GWO achieves the lowest overshoot value (18.12812) compared to CA (22.48623) and HO (30.14214), giving approximately 39.9% reduction. For ΔPtie,2, CA demonstrates superior performance with a minimum overshoot (56.00150) compared to HO (56.95372) and ALO (61.52993). Regarding the ITSE, CA obtains the lowest value (0.70250), outperforming GWO (0.65793) and HO (1.01119) by approximately 30.5% and 43.7%, respectively.

Table 2. The results of scenarios 1

Algorithm	Performance indicators	Δf_1	Δf_2	Δf_3	$\Delta P_{tie,1}$	$\Delta P_{tie,2}$	$\Delta P_{tie,3}$
HO	Overshoot	**0.21411**	**0.13543**	0.10669	30.14214	56.95372	97.18643
	Undershoot	-0.12067	-0.07019	-0.03840	**-142.62085**	-50.40348	-28.34954
	ITSE			1.01119			
GWO	Overshoot	0.21501	0.13963	0.10578	**18.12812**	61.00827	**96.14614**
	Undershoot	-0.11637	-0.06151	-0.02351	-143.13898	-49.79338	**-20.22186**
	ITSE			0.67593			
ALO	Overshoot	0.21506	0.13888	0.10731	19.24644	61.52993	96.98416
	Undershoot	-0.11818	-0.06467	-0.02677	-143.34334	**-48.66205**	-24.13798
	ITSE			0.69488			
CA (proposed)	Overshoot	0.21510	0.13883	**0.10567**	22.48623	**56.00150**	96.49948
	Undershoot	**-0.11498**	**-0.05949**	**-0.01836**	-143.19148	-49.72309	-27.99349
	ITSE			0.70250			

Figure 7 presents the dynamic responses of frequency variations and tie-line power deviations within the three-area interconnected renewable system. Figure 7(a) shows the frequency deviation in Area 1. The California-based controller attains the minimal overshoot and the quickest settling period (about 12 seconds), whereas the HO demonstrates the most significant transient oscillations. GWO and ALO exhibit substantial damping but are less efficacious than CA. Figure 7(b) shows the frequency deviation in Area 2. The CA controller consistently surpasses others with minimum oscillations, attaining around a 25% decrease in overshoot relative to HO. ALO delivers competitive performance, albeit with marginally slower settling

times. Figure 7(c) shows the frequency deviation in Area 3. The system responses exhibit more smoothness owing to the diminished oscillatory characteristics of this region; yet CA demonstrates the least overshoot and enhanced stability compared to alternative methods. Figure 7(d) shows the power variation of the tie-line in Area 1. In this context, CA markedly diminishes oscillations, decreasing amplitude by approximately 40% relative to HO, whereas GWO delivers comparable performance but with slightly extended settling time. Figure 7(e) shows the tie-line power deviation in Area 2, characterized by stronger inter-area oscillations. CA consistently reduces the oscillatory peaks, whereas HO exhibits the most significant and prolonged oscillations. Figure 7(f) shows the tie-line power deviation in Area 3. All algorithms demonstrate diminished oscillation amplitudes relative to other domains; however, CA consistently attains lower deviations, underscoring its durability.

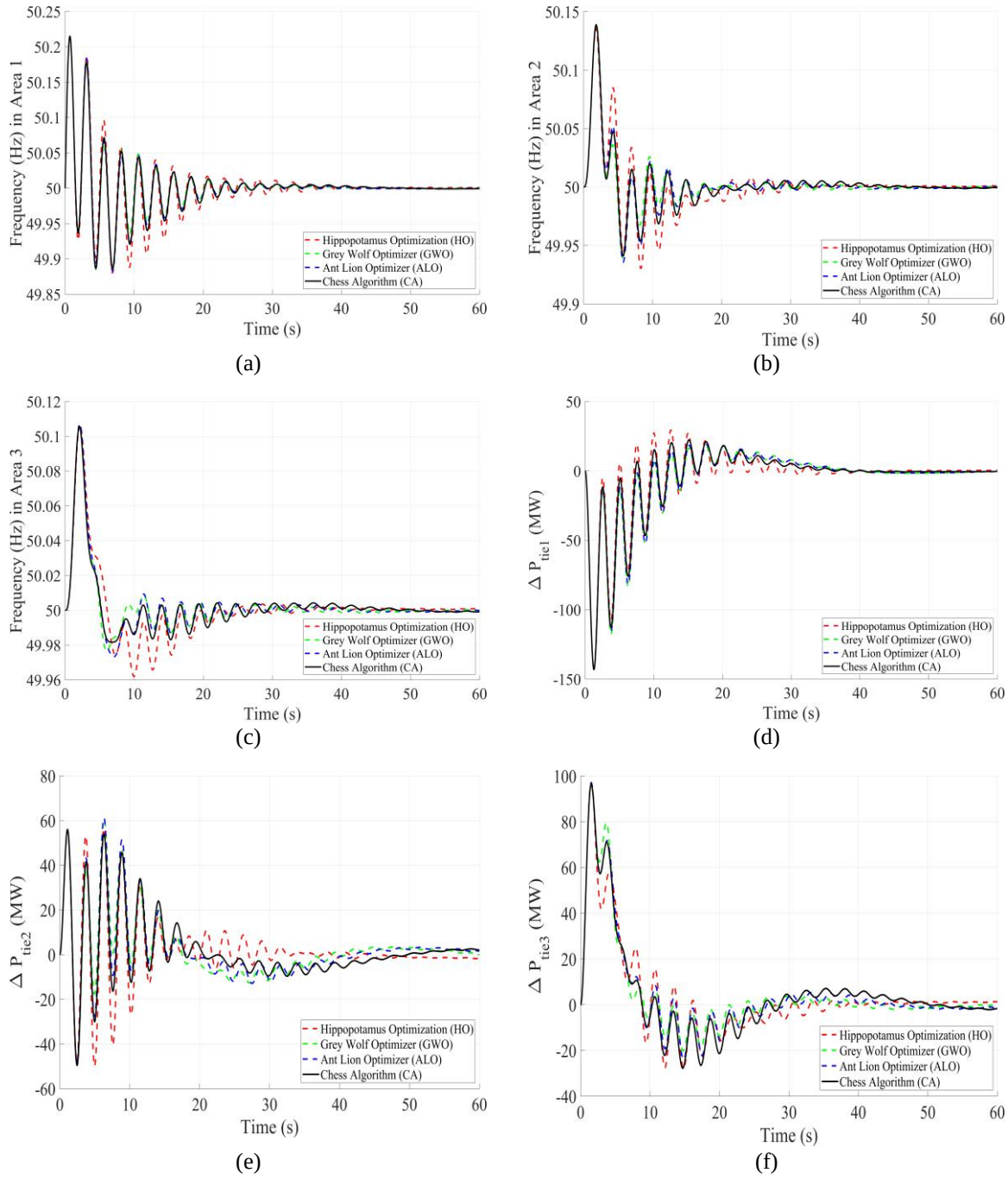

Figure 7. Frequency deviations and tie-line power deviations: (a) variation frequency of Area 1, (b) variation frequency of Area 2, (c) variation frequency of Area 3 (d) power tie-line of Area 1, (e) power tie-line of Area 2, and (f) power tie-line of Area 3

Table 3 lists the optimum controller parameters obtained from the four algorithms under the 10% SLP scenario. The proposed CA yields generally lower values of K_{p1}, K_{i1}, K_{d1} compared to HO, GWO, and ALO, indicating a more balanced PID tuning strategy. For example, the integral gain K_{i1} of CA is 0.2793, which is about 21.3% lower than HO (0.3549) and 16.4% lower than ALO (0.3443). This lower integral action helps suppress overshoot and ensures faster damping, as observed in Figure 7(a). Similarly, the derivative gains, such as K_{d2} and K_{d3}, the values of K_{d3} from CA are significantly smaller than those from GWO and ALO, which highlights CA's capability to avoid excessive derivative amplification that may induce oscillations. On the other hand, the proportional gains K_{d2} and K_{d3} of CA are moderately higher, which strengthens the system's ability to correct frequency deviations rapidly. These parameter patterns explain why CA achieves the lowest ITSE and improved transient stability in scenario 1.

Table 3. Optimum values of algorithm for scenario 10% SLP

	Hippopotamus optimization	Grey wolf optimizer	Ant lion optimizer	Chess algorithm (proposed)
K_{P1}	0.11180	0.01210	0.01044	0.00186
K_{I1}	0.35499	0.23349	0.24429	0.27983
K_{D1}	0.67828	0.61313	0.05219	0.28700
K_{DD1}	0.07835	0.01695	0.10479	0.05630
K_{P2}	0.01348	0.00417	0.05449	0.01001
K_{I2}	0.08230	0.88177	0.70861	0.46086
K_{D2}	0.64087	0.39877	0.48371	0.53590
K_{DD2}	0.25497	0.65787	0.56717	0.08612
K_{P3}	0.42850	0.98874	0.72880	0.92785
K_{I3}	0.06390	0.75821	0.49429	0.52974
K_{D3}	0.78473	0.39216	0.19086	0.88108
K_{DD3}	0.38596	0.92928	0.02738	0.44761

3.2. Scenario 2: random load pattern

Figure 8 presents the dynamic responses in scenario 2. Figure 8(a) shows the frequency deviation in Area 1. The California-based controller attains the minimal overshoot and the swiftest recovery, stabilizing in around 20 seconds following the second disturbance, whereas the higher-order controller exhibits the most significant oscillations with extended settling time. GWO delivers competitive outcomes, albeit with a minor delay in stabilizing. Figure 8(b) shows the frequency deviation in Area 2. CA exhibits robust damping capabilities, diminishing oscillation amplitude by approximately 35% relative to HO, whereas ALO demonstrates considerable suppression; however, residual oscillations endure beyond 40 seconds. Figure 8(c) shows the frequency deviation in Area 3. Despite the naturally smaller oscillations in this region, CA consistently delivers a smoother recovery with less deviation, surpassing HO and ALO, although GWO attains comparable stability with a somewhat extended settling time. Figure 8(d) shows the power variation of the tie-line in Area 1. CA markedly diminishes oscillations, constraining peak deviation to around ±8 MW, whereas HO displays fluctuations above ±12 MW. This underscores CA's efficacy in inter-area oscillation regulation. The tie-line power deviation in Area 2 prominently displays inter-area coupling effects, as shown in Figure 8(e). CA consistently has the minimal oscillation amplitude and the swiftest damping, whereas HO displays the most pronounced transient behavior. Figure 8(f) shows the tie-line power deviation in Area 3. All controllers attain diminished oscillation levels compared to other regions; nevertheless, CA continuously excels with lower amplitudes and expedited stabilization, hence affirming its resilience under recurrent perturbations.

Table 4 provides the optimal parameters for the random load pattern scenario. Again, the CA-derived parameters reveal a balanced tuning profile, with relatively small integral and derivative gains compared to other algorithms. For instance, the integral gain K_{i2} under CA is 0.3905, which is lower than ALO (0.5186) and HO (0.4344), reflecting CA's ability to reduce long-term error accumulation and achieve faster settling following successive disturbances see Figures 8(b) and (e). Moreover, the derivative gain K_{d3} from CA is 0.4869, substantially smaller than GWO (0.9239), thereby avoiding oscillatory spikes that appear in GWO responses. Meanwhile, proportional gains such as K_{p1} and K_{p3} are maintained at moderate levels, ensuring sufficient responsiveness without destabilization. This careful balance across K_p, K_i, and K_d parameters account for CA's superior robustness and adaptability under multiple disturbances, leading to consistent improvements in both frequency regulation and tie-line power stabilization.

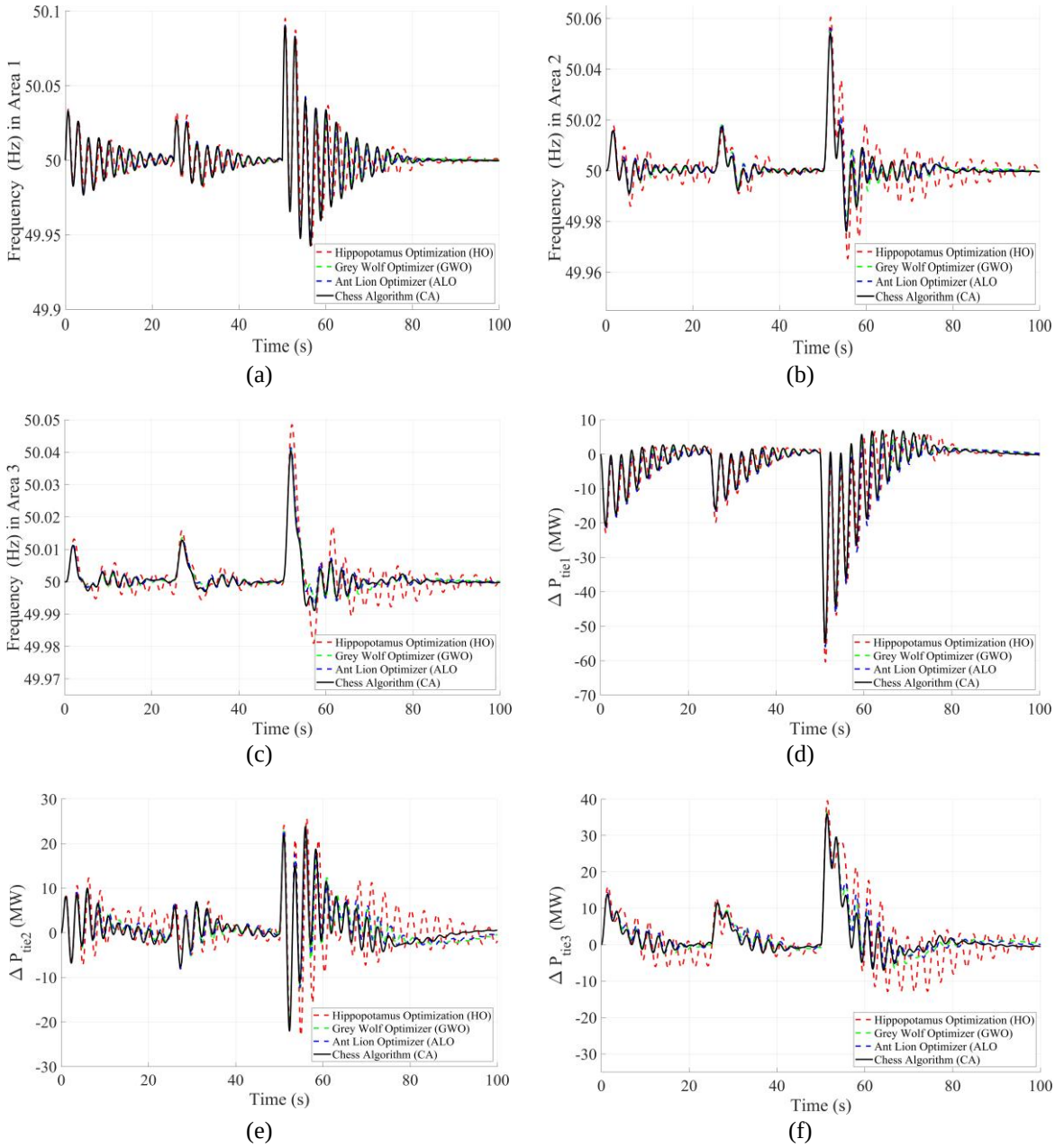

Figure 8. Frequency deviations and tie-line power deviations: (a) variation frequency of Area 1, (b) variation frequency of Area 2, (c) variation frequency of Area 3, (d) power tie-line of Area 1, (e) power tie-line of Area 2, and (f) power tie-line of Area 3

Table 4. Optimum values of algorithm for scenario 2 random load pattern

	HO	GWO	ALO	CA (proposed)
K_{P1}	0.10578	0.40271	0.41621	0.00457
K_{I1}	0.19706	0.19997	0.17846	0.22925
K_{D1}	0.76948	0.76075	0.70667	0.05557
K_{DD1}	0.04193	0.27809	0.68367	0.10197
K_{P2}	0.35910	0.00558	0.23510	0.02591
K_{I2}	0.15070	0.50767	0.60035	0.68868
K_{D2}	0.63440	0.15120	0.27286	0.48388
K_{DD2}	0.43845	0.60239	0.72095	0.54932
K_{P3}	0.04810	0.98871	0.85891	0.74209
K_{I3}	0.55953	0.49793	0.52175	0.50783
K_{D3}	0.05302	0.38832	0.34309	0.21313
K_{DD3}	0.02607	0.09787	0.48698	0.03117

4. CONCLUSION

This paper has presented the application of a PID+DD controller optimized by the CA for load frequency control in a three-area multi-source power system. Comparative analysis under two scenarios—10% SLP and RLP—demonstrates that the proposed CA-based approach consistently outperforms HO, GWO, and ALO. In scenario 1, CA achieves an ITSE of 0.7025, yielding an improvement of 30.5% compared to GWO (0.6759) and 43.7% compared to HO (1.0112). Moreover, CA reduces the frequency undershoot in Area 2 by 15.2% compared to HO and suppresses tie-line oscillations in Area 1 by nearly 40% relative to HO. In scenario 2, CA demonstrates superior robustness, limiting tie-line power deviations to ±8 MW, while HO exhibits deviations beyond ±12 MW. These improvements highlight CA's capability to provide faster damping, lower overshoot and undershoot, and enhanced stability across interconnected renewable power networks.

In summary, the proposed CA-tuned PID+DD controller offers a reliable and effective solution for load frequency stabilization in multi-area hybrid systems. Future work will focus on extending the approach to systems with higher renewable penetration, incorporating energy storage integration, and validating the algorithm under real-time implementation conditions. Such efforts are expected to further establish the CA as a practical and scalable optimization framework for modern renewable-based power systems.

FUNDING INFORMATION

This research project was financially supported by Mahasarakham University.

AUTHOR CONTRIBUTIONS STATEMENT

This journal uses the Contributor Roles Taxonomy (CRediT) to recognize individual author contributions, reduce authorship disputes, and facilitate collaboration.

Name of Author	C	M	So	Va	Fo	I	R	D	O	E	Vi	Su	P	Fu
Chatmongkol Areeyat	✓			✓	✓	✓	✓	✓	✓	✓			✓	✓
Sittihsak Audomsi	✓	✓	✓	✓	✓	✓	✓	✓	✓	✓	✓			
Jagraphon Obma	✓		✓	✓		✓	✓			✓		✓		
Xiaoqing Yang		✓		✓	✓					✓				
Worawat Sa-ngiamvibool	✓	✓		✓	✓	✓	✓	✓	✓	✓	✓	✓	✓	✓

C : **C**onceptualization
M : **M**ethodology
So : **So**ftware
Va : **Va**lidation
Fo : **Fo**rmal analysis
I : **I**nvestigation
R : **R**esources
D : **D**ata Curation
O : Writing - **O**riginal Draft
E : Writing - Review & **E**diting
Vi : **Vi**sualization
Su : **Su**pervision
P : **P**roject administration
Fu : **Fu**nding acquisition

CONFLICT OF INTEREST STATEMENT

The authors declare no conflict of interest.

DATA AVAILABILITY

There is no data which used for this study.

REFERENCES

[1] Mamta, V. P. Singh, A. V. Waghmare, V. P. Meena, F. Benedetto, and T. Varshney, "Rank Exponent Method Based Optimal Control of AGC for Two-Area Interconnected Power Systems," *IEEE Access*, vol. 12, pp. 35571–35585, 2024, doi: 10.1109/ACCESS.2024.3373043.

[2] S. Mishra, P. H. Kumar, R. Ramasamy, R. E. Nambiar, and P. Puvvada, "Load frequency control of interconnected power system using cuckoo search algorithm," *Bulletin of Electrical Engineering and Informatics*, vol. 13, no. 3, pp. 1465–1474, Jun. 2024, doi: 10.11591/eei.v13i3.6714.

[3] S. A. Kumar, M. S. S. N. Varma, and K. J. Gowd, "Load frequency control of multi area system under deregulated environment using artificial gorilla troops optimization," *Bulletin of Electrical Engineering and Informatics*, vol. 11, no. 6, pp. 3051–3060, Dec. 2022, doi: 10.11591/eei.v11i6.4188.

[4] M. Raju, L. C. Saikia, and N. Sinha, "Automatic generation control of a multi-area system using ant lion optimizer algorithm based PID plus second order derivative controller," *International Journal of Electrical Power and Energy Systems*, vol. 80, pp. 52–63, Sep. 2016, doi: 10.1016/j.ijepes.2016.01.037.
[5] C. Tan *et al.*, "Multi-area automatic generation control scheme considering frequency quality in southwest China grid: Challenges and solutions," *IEEE Access*, vol. 8, pp. 199813–199828, 2020, doi: 10.1109/ACCESS.2020.3035067.
[6] A. Daraz, S. A. Malik, H. Mokhlis, I. U. Haq, G. F. Laghari, and N. N. Mansor, "Fitness Dependent Optimizer-Based Automatic Generation Control of Multi-Source Interconnected Power System with Non-Linearities," *IEEE Access*, vol. 8, pp. 100989–101003, 2020, doi: 10.1109/ACCESS.2020.2998127.
[7] S. Panda and N. K. Yegireddy, "Automatic generation control of multi-area power system using multi-objective non-dominated sorting genetic algorithm-II," *International Journal of Electrical Power and Energy Systems*, vol. 53, no. 1, pp. 54–63, Dec. 2013, doi: 10.1016/j.ijepes.2013.04.003.
[8] Z. Huo and C. Xu, "Joint non-fragile automatic generation control and multi-event driven mechanism co-design for wind integrated power system under denial of services attacks," *ISA Transactions*, vol. 150, pp. 148–165, Jul. 2024, doi: 10.1016/j.isatra.2024.04.033.
[9] V. P. Meena, V. P. Singh, and J. M. Guerrero, "Investigation of reciprocal rank method for automatic generation control in two-area interconnected power system," *Mathematics and Computers in Simulation*, vol. 225, pp. 760–778, Nov. 2024, doi: 10.1016/j.matcom.2024.06.007.
[10] Institute of Electrical and Electronics Engineers, "IEEE Recommended Practice for Emergency and Standby Power Systems for Industrial and Commercial Applications," *IEEE Std 446-1995 [The Orange Book]*, vol. 1995. IEEE, Piscataway, NJ, USA, pp. 1–320, Dec. 1996, doi: 10.1109/IEEESTD.1996.85950.
[11] M. H. Amiri, N. M. Hashjin, M. Montazeri, S. Mirjalili, and N. Khodadadi, "Hippopotamus optimization algorithm: a novel nature-inspired optimization algorithm," *Scientific Reports*, vol. 14, no. 1, p. 5032, Feb. 2024, doi: 10.1038/s41598-024-54910-3.
[12] S. Mirjalili, S. M. Mirjalili, and A. Lewis, "Grey Wolf Optimizer," *Advances in Engineering Software*, vol. 69, pp. 46–61, Mar. 2014, doi: 10.1016/j.advengsoft.2013.12.007.
[13] S. Mirjalili, "The ant lion optimizer," *Advances in Engineering Software*, vol. 83, pp. 80–98, May 2015, doi: 10.1016/j.advengsoft.2015.01.010.
[14] S. Audomsi *et al.*, "The development of pid controller by chess algorithm," *Engineering Access*, vol. 10, no. 1, pp. 46–50, 2024, doi: 10.14456/mijet.2024.6.
[15] S. M. Alshareef, "Random subspace ensemble-based detection of false data injection attacks in automatic generation control systems," *Heliyon*, vol. 10, no. 20, p. e38881, Oct. 2024, doi: 10.1016/j.heliyon.2024.e38881.
[16] R. K. Khadanga, A. Kumar, and S. Panda, "Frequency control in hybrid distributed power systems via type-2 fuzzy PID controller," *IET Renewable Power Generation*, vol. 15, no. 8, pp. 1706–1723, Jun. 2021, doi: 10.1049/rpg2.12140.
[17] A. Sharma and N. Singh, "Load frequency control of connected multi-area multi-source power systems using energy storage and lyrebird optimization algorithm tuned PID controller," *Journal of Energy Storage*, vol. 100, p. 113609, Oct. 2024, doi: 10.1016/j.est.2024.113609.
[18] S. Ekinci, O. Can, M. S. Ayas, D. Izci, M. Salman, and M. Rashdan, "Automatic Generation Control of a Hybrid PV-Reheat Thermal Power System Using RIME Algorithm," *IEEE Access*, vol. 12, pp. 26919–26930, 2024, doi: 10.1109/ACCESS.2024.3367011.
[19] T. Ali *et al.*, "Terminal Voltage and Load Frequency Control in a Real Four-Area Multi-Source Interconnected Power System with Nonlinearities via OOBO Algorithm," *IEEE Access*, vol. 12, pp. 123782–123803, 2024, doi: 10.1109/ACCESS.2024.3453755.
[20] A. Hassan, M. M. Aly, A. Selim, A. Elmelegi, A. O. Aldhaibani, and E. A. Mohamed, "Optimal cascade 2DOF fractional order master-slave controller design for LFC of hybrid microgrid systems with EV charging technology," *Results in Engineering*, vol. 25, p. 103647, Mar. 2025, doi: 10.1016/j.rineng.2024.103647.
[21] K. P. S. Parmar, S. Majhi, and D. P. Kothari, "Load frequency control of a realistic power system with multi-source power generation," *International Journal of Electrical Power and Energy Systems*, vol. 42, no. 1, pp. 426–433, Nov. 2012, doi: 10.1016/j.ijepes.2012.04.040.
[22] W. Sa-ngiamvibool, "Optimal Fuzzy Logic Proportional Integral Derivative Controller Design by Bee Algorithm for Hydro-Thermal System," *IEEE Transactions on Industrial Informatics*, pp. 1–1, 2023, doi: 10.1109/TII.2017.2647812.
[23] H. H. Coban, A. Rehman, and M. Mousa, "Load Frequency Control of Microgrid System by Battery and Pumped-Hydro Energy Storage," *Water (Switzerland)*, vol. 14, no. 11, p. 1818, Jun. 2022, doi: 10.3390/w14111818.
[24] G. Magdy, E. A. Mohamed, G. Shabib, A. A. Elbaset, and Y. Mitani, "SMES based a new PID controller for frequency stability of a real hybrid power system considering high wind power penetration," *IET Renewable Power Generation*, vol. 12, no. 11, pp. 1304–1313, Aug. 2018, doi: 10.1049/iet-rpg.2018.5096.
[25] M. Khamies, G. Magdy, M. E. Hussein, F. A. Banakhr, and S. Kamel, "An Efficient Control Strategy for Enhancing Frequency Stability of Multi-Area Power System Considering High Wind Energy Penetration," *IEEE Access*, vol. 8, pp. 140062–140078, 2020, doi: 10.1109/ACCESS.2020.3012119.
[26] G. Magdy, G. Shabib, A. A. Elbaset, and Y. Mitani, "Renewable power systems dynamic security using a new coordination of frequency control strategy based on virtual synchronous generator and digital frequency protection," *International Journal of Electrical Power and Energy Systems*, vol. 109, pp. 351–368, Jul. 2019, doi: 10.1016/j.ijepes.2019.02.007.

APPENDIX A

The parameters of the system are f=50 Hz, n=100, D_{pi}=0.01 p.u, D_{fi}=1 Hz, D_i=0.01 p.u. MW/Hz, H_i=5 sec, R_i=p.u. Hz/MW, B_i=0.4267 p.u. Hz/MW, K_{pi}=100 Hz/p.u. MW, T_{pi}=20 sec, T_{ij}=0.0707 p.u. MW/rad, a_{12}=-1/2, a_{13}=-1/4, a_{23}=-1/2, T_{g1}=0.08 sec, T_{t1}=0.4, K_{r1}=0.33, T_{r1}=10 sec, T_{h1}=48.7 sec, T_{h2}=5, T_{h3}=0.513 sec, T_w=1, T_{g3}=0.08 sec, T_{t3}=0.4, K_{r3}=0.33, T_{r3}=10 sec; normal loading 10%.

BIOGRAPHIES OF AUTHORS

Chatmongkol Areeyat currently pursuing a M.Eng. in the Faculty of Engineering major of Electrical and Computer Engineering. He obtained a B.Eng. degree in Electrical Engineering the Faculty of Engineering at Mahasarakham University in 2024. He focuses on research in the fields of control systems, optimization methods, algorithms, and artificial intelligence. He can be contacted at email: 67010353011@msu.ac.th.

Sitthisak Audomsi currently pursuing a Ph.D. in the Department of Electrical and Computer Engineering. Received the B.Eng. degree in Electrical Engineering in 2023 and the M.Eng. degree in Electrical and Computer Engineering in 2024, both from Mahasarakham University (MSU), Maha Sarakham, Thailand, where he is currently pursuing the Ph.D. degree in Electrical and Computer Engineering. His research interests include control systems, optimization methods, and artificial intelligence. He can be contacted at email: sitthisak.seagame@gmail.com.

Jagraphon Obma obtained a B.Sc. in computer technology from Rajamangala University of Technology Thanvaburi, followed by an M.Eng. and Ph.D. in electrical and computer engineering from Maha Sarakham University (MSU), Thailand. His research interests encompass dual-sided interdigital capacitor sensors. Since 2023, he has been affiliated with the Department of Mechatronics Engineering at Rajamangala University of Technology ISAN, Khonkaen Campus, Thailand, where he presently serves as a lecturer in electrical engineering. He can be contacted at email: Jagraphon.ob@rmuti.ac.th.

Xiaoqing Yang currently pursuing a Ph.D. in the Department of Electrical and Computer Engineering at Mahasarakham University, Mahasarakham, Thailand. In addition to her studies, she work as a lecturer at Shanxi Vocational University of Engineering Science and Technology in Taiyuan, Shanxi, China. Her research focuses on big data technology, machine learning algorithms, encrypted traffic identification, and anomaly detection technology. She can be contacted at email: yangxqmty0907@163.com.

Worawat Sa-ngiamvibool received his B.Eng. degree in Electrical Engineering, the M.Eng. degree in Electrical Engineering from the Khonkaen University (KKU), Thailand and the Ph.D. degree in Engineering from Sirindhorn International Institute of Technology (SIIT), Thammasat University, Thailand. His research interests include analog circuits and power systems. Since 2007, he has been with Faculty of Engineering, Mahasarakham University (MSU), Thailand, where he is currently a Professor of Electrical Engineering. He can be contacted at email: wor.nui@gmail.com.